ACS SENSORS

Article

pubs.acs.org/acssensors

Biofouling Removal and Protein Detection Using a Hypersonic Resonator

Shuting Pan,[†,#] Hongxiang Zhang,[‡,#] Wenpeng Liu,[†] Yanyan Wang,[†] Wei Pang,[*,‡] and Xuexin Duan[*,†]

[†]State Key Laboratory of Precision Measuring Technology & Instruments and [‡]College of Precision Instrument and Opto-electronics Engineering, Tianjin University, Tianjin 300072, China

Supporting Information

ABSTRACT: Nonspecific binding (NSB) is a general issue for surface based biosensors. Various approaches have been developed to prevent or remove the NSBs. However, these approaches either increased the background signals of the sensors or limited to specific transducers interface. In this work, we developed a hydrodynamic approach to selectively remove the NSBs using a microfabricated hypersonic resonator with 2.5 gigahertz (GHz) resonant frequency. The high frequency device facilitates generation of multiple controlled microvortexes which then create cleaning forces at the solid−liquid interfaces. The competitive adhesive and cleaning forces have been investigated using the finite element method (FEM) simulation, identifying the feasibility of the vortex-induced NSB removal. NSB proteins have been selectively removed experimentally both on the surface of the resonator and on other substrates which contact the vortexes. Thus, the developed hydrodynamic approach is believed to be a simple and versatile tool for NSB removal and compatible to many sensor systems. The unique feature of the hypersonic resonator is that it can be used as a gravimetric sensor as well; thus a combined NSB removal and protein detection dual functional biosensor system is developed.

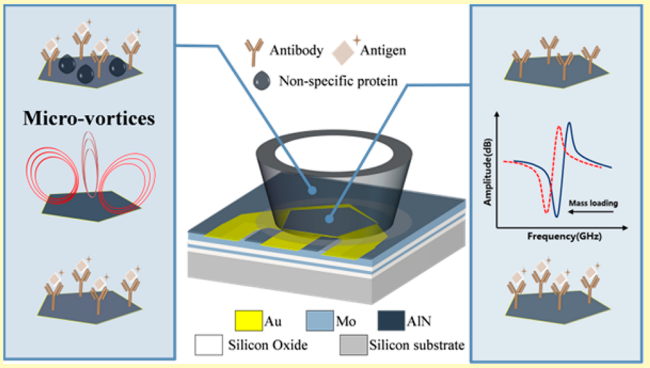

KEYWORDS: *biosensor, hypersonic resonator, nonspecific binding, gravimetric sensor, protein detection*

Quantitative detection of low-abundance proteins (e.g., biomarkers) is the central goal of modern biosensors.[1−3] Various types of affinity biosensors have been developed to this end including surface plasmon resonance (SPR),[4] quartz crystal microbalance (QCM),[5] field-effect transistors (FETs),[6] and electrochemical sensors.[7] These sensors rely on the fidelity of affinity interactions between surface-bound probes and their target proteins to produce an assay signal specific to analyte. One of the major concerns regarding these surface-capture biosensors is the protein nonspecific binding (NSB) or biofouling in many reports, which means that any protein present in solution will tend to bind to the biosensor's surface, thus leading to high background signals that cannot be differentiated from the intended specific binding. NSB is attributed to the fact that proteins can adsorb to the sensor surface through electrostatic, van der Waals, and Lewis acid−base forces as well as through hydrophobic interactions and conformational changes;[8] therefore NSB is ubiquitous and inevitable in surface based biosensors. With respect to the impact of NSB in protein detection, it was elucidated and estimated in mathematic models,[9,10] and otherwise in experimental observations, and concludes that the effects of NSB result in false-positive signals and play a vital role in the limit of detection (LOD), selectivity, sensitivity, and reproducibility of biosensors.[11,12]

Various chemical approaches have been developed to suppress the protein NSB.[13] These approaches include the blocking of reactive surface sites by the addition of blocking agents such as the protein bovine serum albumin (BSA), skim milk powder, or other reagents and the presence of surfactants such as Tween-20 and sodium dodecyl sulfate (SDS) during the sensing.[14] Coating the sensor surface with chemically synthesized polymers or thin films, such as fluorocarbon polymers,[15] polyethylene glycol,[16] poly(vinyl alcohol),[17] polyelectrolytes,[18] zwitterionic polymers,[19] and functionalized self-assembled monolayers (SAMs),[20] has been applied to minimize the NSB as well. The basic principle of these approaches is creating a thin hydrophilic and noncharged interface layer to resist protein adsorption. However, these methods are confronted with the challenges of the tedious functionalization processes, intrinsically increasing the sensor background signal, long-term chemical stability, and the possibility to degrade the active surface. Other than chemical approaches, physical methods using active forces to remove protein NSBs recently have emerged as promising technologies. These approaches are based on the use of different types of transducers to generate surface shear or body forces which are

Received: May 5, 2017
Accepted: July 21, 2017
Published: July 21, 2017

DOI: 10.1021/acssensors.7b00298
ACS Sens. XXXX, XXX, XXX−XXX

stronger than the adhesive force of nonspecific absorbed proteins, and thus they can selectively remove the loosely absorbed proteins.[21] The transducers can be mainly classified as electromechanical[22,23] and acoustic devices.[24,25] The physical NSB removal methods can be applied for various kinds of proteins, making them candidates for time-saving, easy operating, and efficient approaches for removing NSB. However, the cleaning forces all arise from the electrical or mechanical vibration of the devices. Thus, the NSB removal effects of these physical approaches are limited to the proteins which adsorbed on the transducer surface.

To solve these issues, here, we demonstrated a novel NSB removal approach using controlled fluid motion induced by a microfabricated gigahertz hypersonic resonator. Due to its rather high resonance frequency, a hypersonic resonator can directly produce efficient microvortexes in liquid, which result from the attenuation of acoustic energy into liquid.[26] These vortexes will induce the drag forces on the loosely surface-bound proteins lying on the interfaces between the vortexes and the substrates, and thus the technique can be easily applied to many types of microarrays and surface-based biosensors. In this work, we characterized and discussed the mechanism of the microvortexes and the induced removal forces with a finite element model (FEM). The biofouling removal is experimentally proven by removing the nonspecific surface-bound proteins both on the device surface and on substrates in contact with the vortexes through the liquid. Due to the fact that the resonator can be used as a gravimetric sensor to detect the molecular interactions through the mass loading effect,[27−29] we have finally demonstrated a combined biosensing/NSB removal dual functional biosensor system with high selectivity and efficiency.

EXPERIMENTAL SECTION

Reagents and Materials. (3-Aminopropyl) triethoxysilane (APTES), Tween-20 and 3 μm polystyrene particles were obtained from Aladdin (Shanghai, China). 1,4-Phenylene diisothiocyanate (PDC) was obtained from J&K Scientific (Beijing, China). Bovine serum albumin (BSA), human IgG antibody, mouse immunoglobulin G (IgG) antigen labeled by FITC, and human IgG antigen labeled by Cy3 were purchased from Beijing Biosynthesis Biotechnology. All chemicals were of analytical reagent grade and used without extra purification.

Device Fabrication. The device is fabricated using a complementary metal oxide semiconductor (CMOS) compatible technology, and the fabrication process can be found in previous publications.[30] Briefly, thin layers of aluminum nitride (AlN) and silicon dioxide (SiO_2) were alternatively deposited on a silicon substrate, which is configured as Bragg reflector layers. Then, 200 nm molybdenum (Mo), 1.1 μm AlN, and 200 nm Mo were deposited and patterned to form the sandwich structures of the hypersonic resonator, followed by the deposition of 200 nm AlN to serve as the passivation and sensing layer. The schematic structure of the device and the photograph of it are shown in Figure S-1.

Protein Immobilization. The substrates were rinsed with deionized water, dried with nitrogen, and treated with oxygen plasma for 1 min, respectively. Amino-terminated monolayer was achieved by vapor deposition of APTES using a heated vacuumed oven (YES LabKote) at 125 °C, 5.2 Torr, for 20 min. Subsequently, the substrates were immersed in 0.01 M PDC solution in ethanol at 65 °C for 1 h to form an isothiocyanate-bearing layer which functioned as a cross-linker to immobilize the proteins. The isothiocyanate-bearing substrates were then incubated in protein solutions for 30 min (typical 100 μg/mL in 1× PBS buffer), and the substrates were then rinsed with 1× PBS buffer. BSA solution of 1 mg/mL in PBS was applied to the substrates to block the unbounded sites, followed by PBS buffer rinsing.

Protein Micropatterns. Poly(methyl methacrylate) (PMMA) (Microchem Corp., A6950) was first applied to pattern microsized circular patterns on device surface typically with diameters of 20 μm (described in Supporting Information Part 4). The exposed surface was allowed for APTES and isothiocyanate functionalization as mentioned above. Acetone was then applied to remove PMMA, leaving the PMMA protected regions unfunctionalized. The substrates were then incubated in protein solutions to form protein micropatterns.

Setups for Biofouling Removal and Protein Sensing. For protein removal, the resonator was actuated by a frequency generator (Agilent N2181B) connected with a power amplifier (Mini-Circuits ZHL) (see Supporting Information Part 2 for a detailed description). For protein detections, the resonator was driven by a vector network analyzer (Agilent N50171C), and the frequency shift was monitored. The video and images of microvortexes in top view are acquired by microscope (Olympus BX53) with a CCD camera (Olympus DP73). The side view is acquired by a contact angle measurement instrument (Powereach JC2000CDM) (see also Supporting Information Part 2). Fluorescence imaging was utilized to characterize the functionalization of antigen and the efficiency of NSB removal. Fluorescence images were post-processed by ImageJ. All the processes were conducted in darkness to avoid the regular light induced fluorescence quenching. Fluorescence images were taken before and after the resonator removal in each experiment.

In the removal experiment, plastic chambers of 50 μm height were sealed on the device substrates. 5 μL of 1× PBS and 5 μL of Tween-20 with 1:1.7 in 1× PBS were dropped into the chamber in sequence. Then, the chamber was covered with a lid. Finally, 500 mW power was applied to the resonator for 10 min (herein referred to as hypersonic treatment) to remove nonspecific bond proteins. In the contactless removal experiment, the lid was replaced by the substrates with protein patterns. As for the removal and sensing experiment, the frequency shift was monitored after each step, and the removal process is repeated as mentioned earlier.

RESULTS AND DISCUSSION

Theory, Characterizations and Simulations of the Microvortexes. The nonlinear effect occurs in fluid due to fluidity, which accounts for the appearance of the nonzero time-averaged term when periodic acoustic wave propagates into fluid, and further results in acoustic radiation force.[31] The radiation force can interact with the fluid media and trigger the acoustic streaming effects.[32] In other words, the generation of acoustic streaming could also be regarded as the acoustic power leakage during the propagation of the acoustic waves into liquid. The acoustic streaming has been reported for enhanced fluid mixing within microfluidic channels,[26] particle concentration,[33] manipulations of micro/nanoparticles,[34] and many other applications according to previous reports.[35,36] Due to the fact that high frequency acoustic waves have a greater energy attenuation coefficient after their transmission into liquid, high frequency acoustic waves will induce higher streaming velocity.[37] In addition, compared with shear mode acoustic waves, wherein the effective energy decay length is below several nanometers and most of the coupled energy is distributed, longitudinal waves can provide more effective energy coupling into liquid due to their longer attenuation length (up to micrometers), so that the acoustic energy is no longer bound to the transducer surface and forms stronger turbulent flow inside the fluids. In this work, we fabricated the hypersonic device with a 2.5 GHz resonance frequency, which can generate longitudinal waves perpendicular to the device substrate. Moreover, the relationship between frequency and viscous boundary thickness (σ) is $\sigma \sim (\mu/2\pi f\rho)^{1/2}$;[38] here, the viscosity and the density of fluid are denoted by μ and ρ, and

DOI: 10.1021/acssensors.7b00298
ACS Sens. XXXX, XXX, XXX−XXX

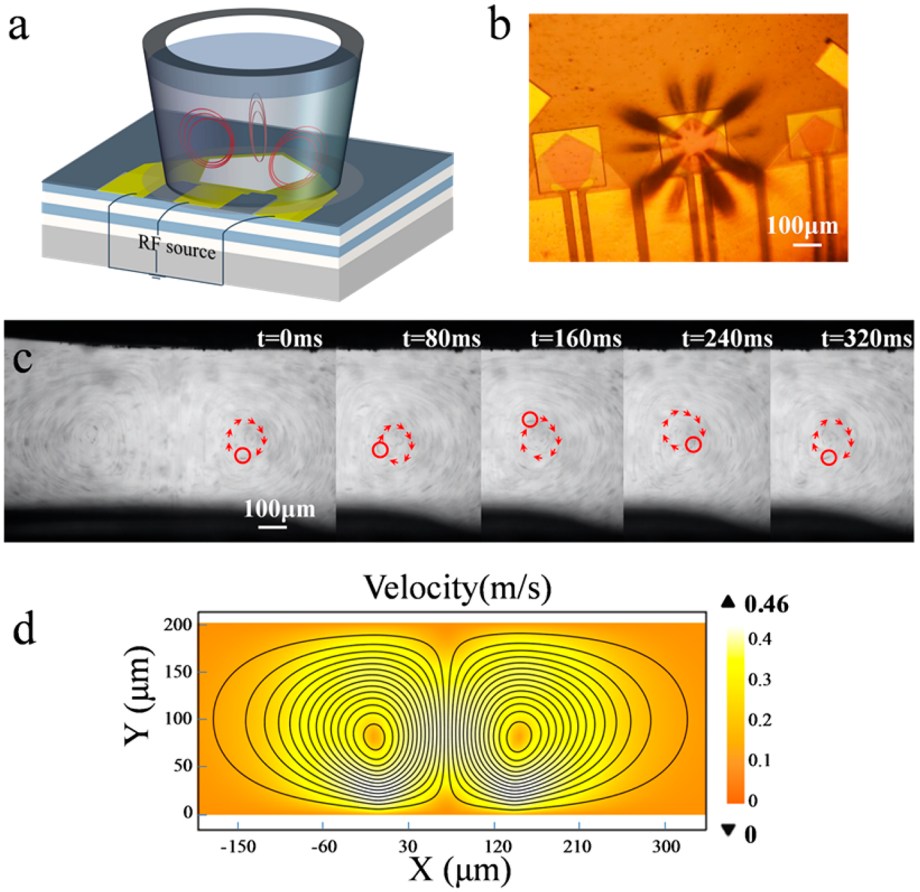

Figure 1. Characterizations and simulations of the microvortexes. (a) Schematic illustration of microvortexes in liquid triggered by the hypersonic resonator. Microscopic images of the microvortexes in top view (b) and side view (c). The trajectory of one particle (red arrows) is formed by tracing the particle (red circles marked) at different times. (d) Simulation of the fluid motion triggered by the hypersonic resonator.

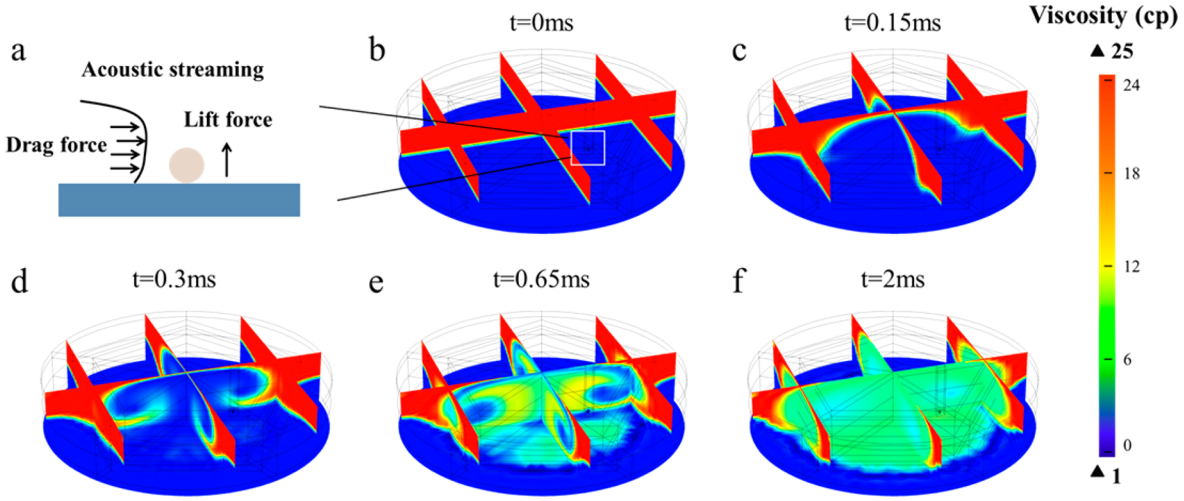

Figure 2. 3D FEM simulation of the time-dependent distributions of the viscosity as well as the flow motions. (a) Schematic of the forces related to NSB surface removal. (b), (c), (d), (e), and (f) show the interactions between vortexes and a particle at different times by the viscosity distributions. Orthogonal cross sections are utilized to facilitate the observations of the internal structure of this 3D simulation.

the acoustic wave frequency is denoted by *f*. Therefore, as for the NSB removing system, increasing frequency will decrease viscous boundary layer;[38] thus, the induced removal force can work on very tiny particles (e.g., proteins) on the sensor surface rather than these particles being hidden in the viscous boundary layer. In brief, the longitudinal wave propagation and high operation frequency enables the hypersonic resonator to be an effective actuator in triggering acoustic streaming and removing NSB proteins.

In order to visualize the fluid motions excited by the hypersonic resonator, we used 3 μm polystyrene particles to facilitate the observations of the microvortexes. 20 mW power was applied to the hypersonic resonator to trigger microvortexes with low velocity which facilitates the imaging. Figure

DOI: 10.1021/acssensors.7b00298
ACS Sens. XXXX, XXX, XXX−XXX

1b,c shows the top and side views of the microvortexes respectively (complete videos can be found in the Supporting Information). As shown in the figures, there exist ten microvortexes standing on the edge of the resonator surface which can be easily identified by the steam lines of the vortexes. These results indicate that the hypersonic device can generate multiple microvortexes, enabling it as an actuator for stable and effective vortex generation.

The finite element method (FEM) was then applied to reveal the fluid motion induced by the hypersonic resonator in the form of flow velocity. Figure 2d shows the simulation result which indicates that the acoustic radiation force induced by the hypersonic resonator will result in accelerated and upward fluid flow upon the resonator, while the surrounding liquid makes up, thus inducing a localized liquid flow. When the fluid flows at the liquid−air and liquid−solid interfaces (e.g., the resonator or a top cover), the flow velocity fades to zero and then the fluid will be pushed by other fluid elements. Overall, every fluid element upon the hypersonic resonator experiences radiation force by the resonator, interference by interfaces, and traction by fluid movements in succession, and eventually results in the microvortexes around the resonator, which is in good agreement with the experimental observations.

Microvortex-Induced NSB Removal. It is known that the proteins tend to nonspecifically bond to the surface resulting from surface adhesive forces which are due to the hydrophobic nature of the proteins, the electrostatic interactions, as well as van der Waals interactions. In principle, the generated microvortexes can be used to act on these weakly bound proteins. Here, we used a simplified model to analyze the removal forces and compared them with the protein adhesion forces (Figure 2a). Among all the surface adhesion forces, van der Waals (F_{vdW}) force is regarded as the major force to be conquered.[38] The biofoulings to be removed here are considered particles (100 nm), and F_{vdW} is given by

$$F_{vdW} \approx AR/(6z^2) \quad (1)$$

Here, A is the Hamaker constant, R is the radius for the particle to be removed, and z is the adhesion distance. The calculated F_{vdW} is about 2×10^{-9} N.

With respect to removal force, the interactions between fluid and the hypersonic resonator mainly lead to lift force (F_L) and drag force (F_S). Lift force (F_L) is due to a pressure difference between the upper and lower surfaces of the particle when fluid flows through it, and the direction of it is normal to the substrate. It can be described in eq 2, where ρ refers to the density of the liquid and u_x is the surface normal component of velocity.

$$F_L \approx \rho(u_x R)^2 \quad (2)$$

Drag force (F_S) mainly results from the effect of acoustic streaming induced mean flow on the particle, which, in other words, is the product of vortex motion. This force can be described by eq 3,[39] from which μ and u refer to the viscosity of the fluid and the flow velocity, respectively.

$$F_S \approx 6\pi\mu R u \quad (3)$$

In order to investigate the removal system based on microvortexes and optimize the removal conditions, a 3D FEM simulation was used to evaluate the order-of-magnitude forces related to NSB removal (Figure 2b−f).

To study the removal mechanism and explore the optimized condition, we regulated the viscosity of the fluid and finally utilized two liquid layers with different viscosities as removal medium. The liquid layer with low viscosity contributes to maintaining high streaming velocity, while the liquid layer with high viscosity results in effective removal. When the resonator is activated, microvortexes are triggered, and then two liquid layers will be perturbed according to the flow motion. At the same time, these two layers will interact with each other (here manifested as mutual solubility), and thus the viscosity distribution of the liquid changes with time until uniformity is reached. The time-dependent distributions of viscosity as well as flow motion are shown in Figure 2b,c,d,e,f (a fully simulated movie can be found in the Supporting Information). We obtained the streaming velocity and fluid viscosity from this 3D mode, and the magnitudes of removing forces are calculated and listed in Supporting Information Part 3. F_S in this condition is $\sim 10^{-9}$ N, which is the same order of magnitude as F_{vdW}, while F_L is the order of magnitude of 10^{-13} N.

According to these results, we conclude that the drag force resulting from the acoustic streaming predominates in biofouling removal on account of its comparable magnitude with the protein adherent force. Moreover, even though we found that the maximum removing force occurs in the process of mutual dissolution between two liquid layers within 2 ms, which is indicated by the simulation, enough removal time is still essential for an efficient removal since the roles of accumulated effects of several fluid circulations are more prominent as the acoustic streaming is a nonzero time average. Besides, by increasing the applied power, the removal force can be further increased to achieve a more effective surface removal. According to the simulation, the proper power for exciting the hypersonic device to remove NSB protein is 2−3 W, while in fact, NSB removal could be efficiently achieved within 500 mW at the sweep-frequency mode, indicating that this simulation is simplified and the real condition is much more complicated. In addition, in the real case, the specific protein bindings should be prevented from destruction by any removal approaches when it comes to NSB removal; therefore, we prefer to apply relatively weak power and long operation time to ensure a controllable and noninvasive NSB removal, especially in the low-affinity binding system. With respect to some extreme conditions, we can regulate the removal system by tuning the input power. Once the particle is pulled a little distance from the surface, a distinct attenuation of van der Waals occurs, and eventually the particle is readily removed. When the particle is released from the device, lift force will prevent its reattachment to the surface, as shown in Figure 2a.

Given that the dominant removal force is the drag force, which mainly depends on the vortexes standing on the hypersonic resonator, and that the flow motion is not significantly different between the top and bottom surface both in practical observations (Figure 1c) and in fluid simulations (Figure 1d), the resulting NSB removal effects can be applied not only on the resonator surface but also on the substrates suspended over the device which contact the vortexes through liquid.

In our numerical and simulation models, NSB proteins are simulated as sphere particles with diameter of 100 nm.[21,40] When simulating the protein size at 1−10 nm, it requires applying very high power (e.g., 5 W) to remove these particles. However, in the NSB removal experiments, relatively low power (500 mW) is effective enough to remove all NSBs. The

DOI: 10.1021/acssensors.7b00298
ACS Sens. XXXX, XXX, XXX−XXX

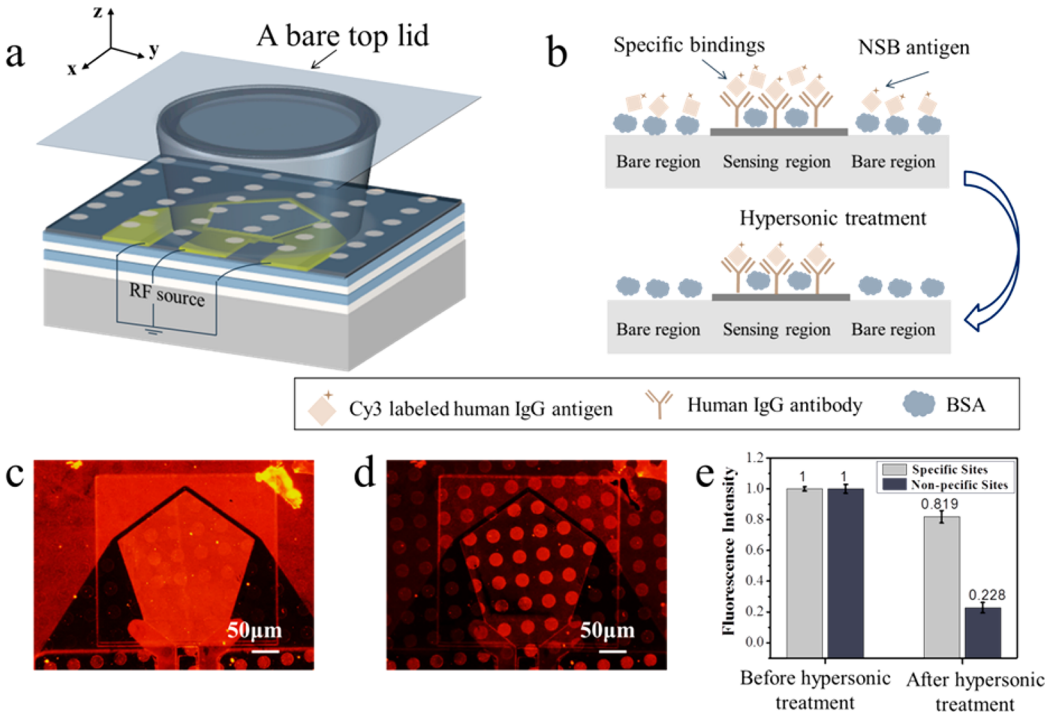

Figure 3. Results of NSB removal on the resonator surface. The schematic of NSB removing setup (a) and the process flow to remove the proteins on the device surface (b). Florescent microscope images of the resonator before (c) and after (d) the hypersonic treatment and their normalized fluorescence intensity data (e).

reason is that the biofouling removal is actually due to synergistic effects induced by the hypersonic resonator. (1) Regarding to the NSB removal on the device surface, besides the drag forces, the hypersonic resonator will generate large body forces which will work on the NSB proteins staying on the resonators. (2) Regarding to the NSB removal on the substrate suspended over the device, the hypersonic resonator will induce high and instantaneous impulsive forces as inferred from the side view of the microvortexes. The impulsive force will change the interface configurations and may further induce intermolecular interactions of these NSB proteins. However, these interface interactions are complicated and difficult to quantify reliably with simple models. Thus, in this work, the simplified numerical model and 3D simulation model are appropriate in revealing the mechanism in removing biofoulings in the size of 0.1−10 μm, while for 1−10 nm particle removal, the device body force and impulsive force-induced interface conversion of NSBs should be taken into consideration.

NSB Removal on Resonator Surface. Figure 3a shows the NSB removal setup. To prevent the unevenly distributed flow which may induce spatial heterogeneity of NSB removal, we design a plastic chamber in the $x-y$ plane within a 3 mm radius from the device center, which is similar to that of 96-well plates, and then this chamber is sealed on top of the resonator; a lid is also included on top of the chamber to confine the solution. Before the NSB removal, we tested different removal conditions by inputting different powers and frequencies (Supporting Information Part 5). We finally selected frequency-sweep excitation and power of 500 mW as the proper input condition to ensure an efficient removal. Other issues relate closely to the experimental strategy are discussed in Supporting Information Parts 6 and 7.

To evaluate the NSB removal effects, protein patterns were created on the resonator surface by photolithography to facilitate the observations. PMMA were first patterned into microarrays on the resonator, followed by surface modification to an isothiocyanate active layer on the opening area. After removing PMMA, antihuman IgGs were then applied to the substrate which will be covalently linked to the surface through amine−isothiocyanate reactions. BSA was utilized to block extra isothiocyanate active layer, and Cy3-labeled human IgG antigen was finally applied to bind antihuman IgGs. Thus, the opening sites would be specific binding sites while other regions previously covered with PMMA would be nonspecific binding areas (Figure 3a,b).

The hypersonic resonator was then excited to trigger vortexes for NSB removal. By generating the surface drag force, the loosely bound NSB proteins were removed from the substrates (Figure 3b). According to the FEM prediction, optimized conditions with two liquid layers can induce more effective drag force, thus the removing process was conducted by dropping 5 μL 1× PBS (the first layer) and 5 μL Tween-20 with 1:1.7 in 1× PBS (the second layer) into the chamber in sequence. Figure 3c,d shows the fluorescence images (both exposed for 100 ms) of the resonator before and after the hypersonic treatment, respectively. Before the removal, the surface is fully covered with Cy3-labeled human IgG antigen, including both specific and nonspecific sites. The specific binding sites are barely recognized. After the hypersonic treatment, the nonspecific binding sites decreased significantly, while specific binding sites kept almost the same; thus the specific protein binding could be clearly identified (Figure 3d), indicating the high efficiency of the NSB removal. The fluorescence images were then post-processed by ImageJ, and the normalized fluorescence intensities are shown in Figure 3e. Before the hypersonic treatment, the mean value of the fluorescence intensity of specific binding sites and nonspecific binding sites are shown in histograms which are almost

DOI: 10.1021/acssensors.7b00298
ACS Sens. XXXX, XXX, XXX−XXX

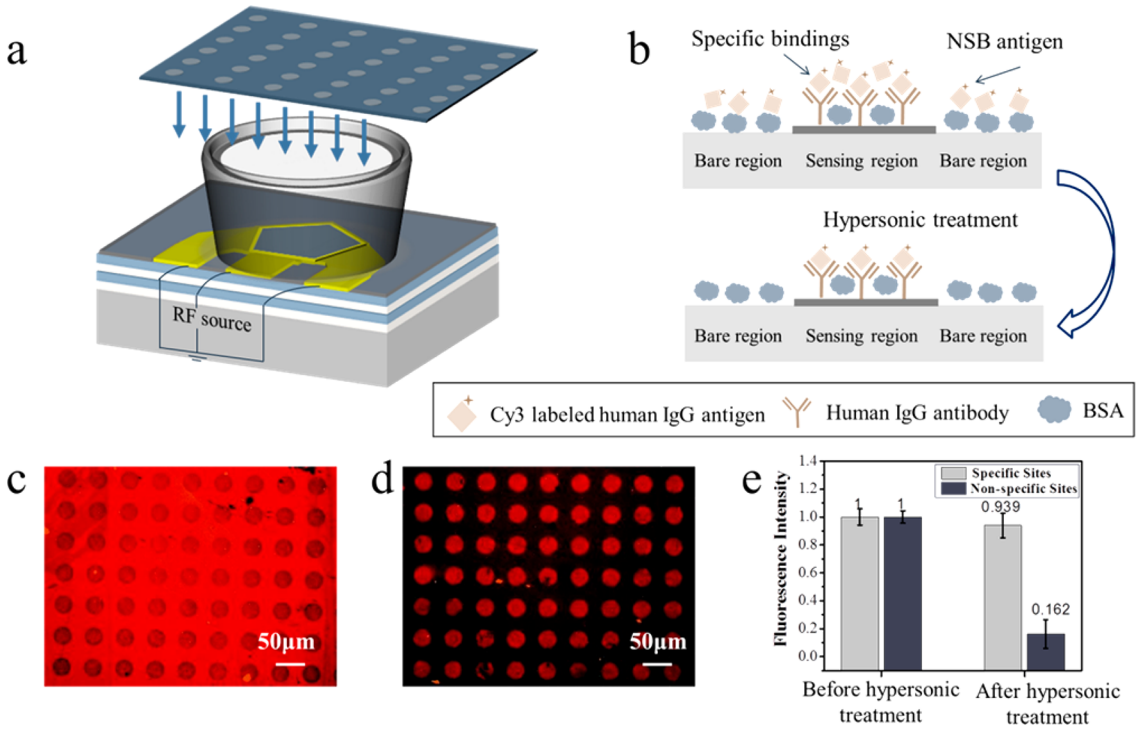

Figure 4. Results of contactless removal. Schematic of contactless NSB removal setup (a) and the process flow to remove the proteins on the top lid (b). Florescent microscopy images of the substrate before (c) and after (d) the hypersonic treatment and their normalized fluorescence intensity data (e).

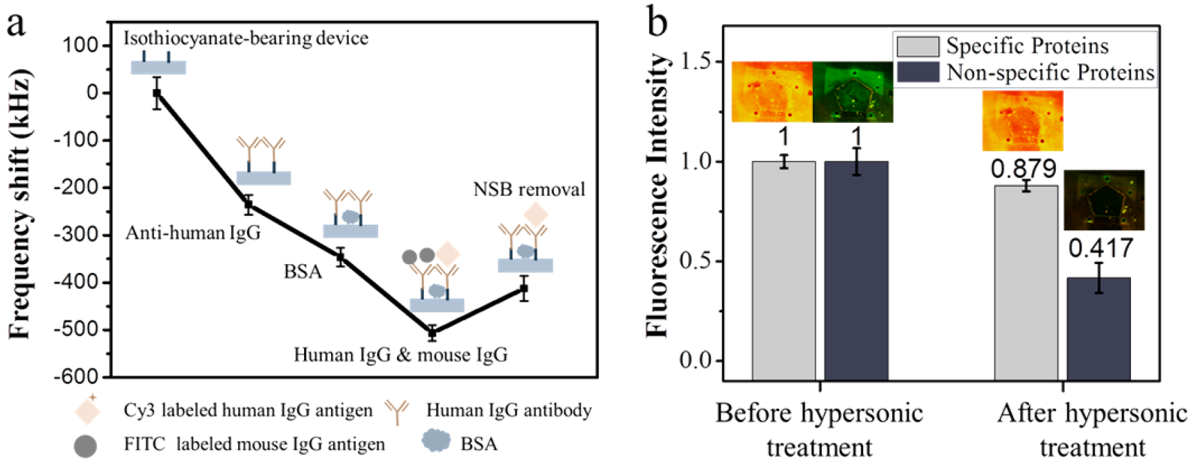

Figure 5. NSB removal and biosensing on the same resonator. (a) Frequency shift corresponding to the change of the mass loading after every modification and the insets shows the schematic. (b) Histogram showing the normalized fluorescence intensity before and after the hypersonic removal, and the corresponding fluorescence images are shown in insets.

equalized. After the treatment, their fluorescence intensity decreased by 18.1% and 77.2%, respectively. The slight disassembling of the specific bond IgGs could be the results of the removal of the overlapping proteins on these regions.

This experiment verified the feasibility of the removal method based on the drag forces induced by the hypersonic acoustic streaming, which agreed well with the theoretical prediction.

Contactless Removal. As explained above, the main driving force of the NSB removal in our system is the drag force induced at the liquid−solid interfaces. Since these vortexes are vertically standing and symmetrically distributed along the edge of the resonators, this opens up the possibility of using this technique to remove the NSB proteins on other substrates which contact the vortexes through the liquid (here referred as contactless removal). Thus, the acoustically triggered vortex system can be employed as a versatile approach for biofouling removal on any other substrates.

To demonstrate this, the bare top lid in Figure 3a was replaced with a patterned protein substrate containing specific and nonspecific binding sites which fabricated similarly to the one on the resonator surface in Figure 3. The solution in the chamber was filled enough to contact the patterned protein chip, and the resonator was actuated to trigger the vortexes and stir the liquid which will flush the nonspecifically bonded IgGs on the top lid (Figure 4a,b).

Figure 4c,d shows the fluorescence images (both exposed for 100 ms) of the patterned protein substrate, before and after the

DOI: 10.1021/acssensors.7b00298
ACS Sens. XXXX, XXX, XXX−XXX

hypersonic removal, respectively. The nonspecific binding sites experienced a significant fluorescence decrease after the treatment, which is due to the effective interactions between the streaming of the vortexes and the infirm bond protein NSB, while the specific binding sites are slightly influenced. The quantitative analysis (Figure 5e) reveals that the fluorescence intensity decreases 6.1% and 83.8% for specific and nonspecific binding sites respectively which demonstrates a similar effect with the direct removal on the resonator surface.

This experiment clearly demonstrates the contactless removal and proves the removal events can be applied to any interfaces between vortexes and solid substrates. Given that large quantities of acoustic energies of the resonator are dissipated into the liquid, any other types of surface based biosensors or microarrays can be suspended over the resonator to employ this strategy to remove the unwanted biofoulings, such as the optical, electrical, and electrochemical biosensors. For this purpose, the hypersonic resonator can serve as a detachable actuator, which allows repeated usage.

Beside the removal results, we carefully characterized the influence of the hypersonic treatment on the bioactivity of the surface bound proteins (see Supporting Information Part 8), from which we conclude that the hypersonic removal method is noninvasive for the bioactivity of the immobilized proteins.

NSB Removal and Biosensing on the Same Resonator. Besides actuating the microvortexes, a unique feature of the hypersonic resonator is that it can be used as a gravimetric sensor as well to detect the surface bound molecules by extracting the frequency changes through the mass loading effect. After demonstration of the NSB removal, we used the resonator to remove the nonspecific bindings in a combined biosensing system. In this system, the resonator acts both as an actuator and as a biosensor, which enabled removal and sensing on the same device.

As the hypersonic resonator is mass-sensitive, the surface process and the removal outcome can be reflected by the shift of the resonance frequency. The resonator was first functionalized with APTES and PDC to active the sensor surface. We used the static measurements to follow the each step of the protein immobilization, BSA passivation, protein sensing, and the NSB removal. Figure 5a shows the biosensing steps and the corresponding resonance frequency shifts. The resonance frequency decreases correspondingly to the addition of antihuman IgG, BSA, and the mixed solutions of Cy3-labeled human IgG and FITC-labeled rabbit IgG with equal concentration of 50 μg/mL in 1× PBS, which proves the successful surface binding of these proteins. After the hypersonic treatment, the resonance frequency is recorded again and it increases by 94 kHz, indicating the removal of the surface bound proteins.

Though the sensor can detect the signals of the disassembly of some proteins, it cannot tell whether the frequency change is due to the removal of human IgG (specific) or mouse IgG (nonspecific). We further identified the results using the fluorescent method. Figure 5b shows the fluorescence images and the corresponding intensities of the resonator surface before and after the hypersonic removal. Cy3 fluorophores and FITC fluorophores were excited by UV light with a wavelength of 550 and 490 nm, respectively (both were exposed for 200 ms). The intensity data was processed by ImageJ and normalized according to the initial fluorescent intensity of the Cy3 fluorophores and FITC fluorophores, respectively. After the hypersonic stimulation, the fluorescence intensity of the mouse IgG decreases 58.3%, while only 12.1% is decreased for human IgG indicating the successful removal of the NSB.

CONCLUSION

Effective methods to remove nonspecific surface bound proteins can enhance the sensor response to targets, which is an essential issue in improving the sensitivity and selectivity of biosensors. In this work, we developed a versatile approach for protein NSB removal using a hypersonic device. The hypersound triggers multiple microvortexes in liquid and generates drag and lift forces in the liquid−solid interfaces which can be used for controlled NSB removal. The mechanism of biofoulings removal is carefully studied with FEM simulations and mathematic models. Experimental results with a designed antibody−antigen binding system were applied to successfully demonstrate the efficient biofouling removal. Significantly, the contactless removal experiment for a suspended substrate over the resonator demonstrated the ability to combine this hypersonic treatment with other surface based biosensors. Because of the ability of the resonator in mass sensing, the hypersonic resonator realized the NSB removal/detection on the same device, demonstrating it as a promising and dual-functional biosensor.

ASSOCIATED CONTENT

Supporting Information

The Supporting Information is available free of charge on the ACS Publications website at DOI: 10.1021/acssensors.7b00298.

Fabrication process of the hypersonic device; experimental setup; the calculation of related forces; fabrication and characterizations of the protein micropatterns; parameters for NSB removal; comparison of removal effect with and without the hypersonic treatment; NSB protein removal using hypersonic treatment without BSA blocking adsorption sites; assessment of the link stability of the antibody to the substrate and the activity of the proteins under hypersonic treatment (PDF)

Top view of microvortexes triggered by the hypersonic resonator (AVI)

Side view of microvortexes triggered by the hypersonic resonator (AVI)

3D FEM simulation of the time-dependent distributions of the viscosity as well as the flow motions (AVI)

AUTHOR INFORMATION

Corresponding Authors

*E-mail: weipang@tju.edu.cn.

*E-mail: xduan@tju.edu.cn.

ORCID

Xuexin Duan: 0000-0002-7550-3951

Author Contributions

#Shuting Pan and Hongxiang Zhang contributed equally.

Notes

The authors declare no competing financial interest.

ACKNOWLEDGMENTS

The authors gratefully acknowledge financial support from the National Natural Science Foundation of China (NSFC No. 51375341, 61674114), the 111 Project (B07014) and the

DOI: 10.1021/acssensors.7b00298
ACS Sens. XXXX, XXX, XXX−XXX

Tianjin Applied Basic Research and Advanced Technology (14JCYBJC41500).

REFERENCES

(1) Lilja, H.; Ulmert, D.; Vickers, A. J. Prostate-specific antigen and prostate cancer: prediction, detection and monitoring. *Nat. Rev. Cancer* **2008**, *8* (4), 268−278.
(2) Isaacs, J. S.; Xu, W.; Neckers, L. Heat shock protein 90 as a molecular target for cancer therapeutics. *Cancer Cell* **2003**, *3* (3), 213−217.
(3) Shangary, S.; Wang, S. Small-molecule inhibitors of the MDM2-p53 protein-protein interaction to reactivate p53 function: a novel approach for cancer therapy. *Annu. Rev. Pharmacol. Toxicol.* **2009**, *49*, 223−241.
(4) Scarano, S.; Mascini, M.; Turner, A. P.; Minunni, M. Surface plasmon resonance imaging for affinity-based biosensors. *Biosens. Bioelectron.* **2010**, *25* (5), 957−966.
(5) Mannelli, I.; Minunni, M.; Tombelli, S.; Mascini, M. Quartz crystal microbalance (QCM) affinity biosensor for genetically modified organisms (GMOs) detection. *Biosens. Bioelectron.* **2003**, *18* (2), 129−140.
(6) Duan, X.; Li, Y.; Rajan, N. K.; Routenberg, D. A.; Modis, Y.; Reed, M. A. Quantification of the affinities and kinetics of protein interactions using silicon nanowire biosensors. *Nat. Nanotechnol.* **2012**, *7* (6), 401−407.
(7) Guo, X.; Kulkarni, A.; Doepke, A.; Halsall, H. B.; Iyer, S.; Heineman, W. R. Carbohydrate-based label-free detection of Escherichia coli ORN 178 using electrochemical impedance spectroscopy. *Anal. Chem.* **2012**, *84* (1), 241−246.
(8) Blawas, A.; Reichert, W. Protein patterning. *Biomaterials* **1998**, *19* (7), 595−609.
(9) Duan, X.; Rajan, N. K.; Izadi, M. H.; Reed, M. A. Complementary metal oxide semiconductor-compatible silicon nanowire biofield-effect transistors as affinity biosensors. *Nanomedicine* **2013**, *8* (11), 1839−1851.
(10) Arlett, J.; Myers, E.; Roukes, M. Comparative advantages of mechanical biosensors. *Nat. Nanotechnol.* **2011**, *6* (4), 203−215.
(11) Zheng, G.; Patolsky, F.; Cui, Y.; Wang, W. U.; Lieber, C. M. Multiplexed electrical detection of cancer markers with nanowire sensor arrays. *Nat. Biotechnol.* **2005**, *23* (10), 1294−1301.
(12) Rissin, D. M.; Kan, C. W.; Campbell, T. G.; Howes, S. C.; Fournier, D. R.; Song, L.; Piech, T.; Patel, P. P.; Chang, L.; Rivnak, A. J. Single-molecule enzyme-linked immunosorbent assay detects serum proteins at subfemtomolar concentrations. *Nat. Biotechnol.* **2010**, *28* (6), 595−599.
(13) Jonkheijm, P.; Weinrich, D.; Schröder, H.; Niemeyer, C. M.; Waldmann, H. Chemical strategies for generating protein biochips. *Angew. Chem., Int. Ed.* **2008**, *47* (50), 9618−9647.
(14) Jeyachandran, Y.; Mielczarski, J.; Mielczarski, E.; Rai, B. Efficiency of blocking of non-specific interaction of different proteins by BSA adsorbed on hydrophobic and hydrophilic surfaces. *J. Colloid Interface Sci.* **2010**, *341* (1), 136−142.
(15) Ko, K.-S.; Jaipuri, F. A.; Pohl, N. L. Fluorous-based carbohydrate microarrays. *J. Am. Chem. Soc.* **2005**, *127* (38), 13162−13163.
(16) Groll, J.; Amirgoulova, E. V.; Ameringer, T.; Heyes, C. D.; Röcker, C.; Nienhaus, G. U.; Möller, M. Biofunctionalized, ultrathin coatings of cross-linked star-shaped poly (ethylene oxide) allow reversible folding of immobilized proteins. *J. Am. Chem. Soc.* **2004**, *126* (13), 4234−4239.
(17) Batra, D.; Vogt, S.; Laible, P. D.; Firestone, M. A. Self-assembled, mesoporous polymeric networks for patterned protein arrays. *Langmuir* **2005**, *21* (23), 10301−10306.
(18) Duan, X.; Mu, L.; Sawtelle, S. D.; Rajan, N. K.; Han, Z.; Wang, Y.; Qu, H.; Reed, M. A. Functionalized Polyelectrolytes Assembling on Nano-BioFETs for Biosensing Applications. *Adv. Funct. Mater.* **2015**, *25* (15), 2279−2286.
(19) Ladd, J.; Zhang, Z.; Chen, S.; Hower, J. C.; Jiang, S. Zwitterionic polymers exhibiting high resistance to nonspecific protein adsorption from human serum and plasma. *Biomacromolecules* **2008**, *9* (5), 1357−1361.
(20) Mrksich, M.; Sigal, G. B.; Whitesides, G. M. Surface plasmon resonance permits in situ measurement of protein adsorption on self-assembled monolayers of alkanethiolates on gold. *Langmuir* **1995**, *11* (11), 4383−4385.
(21) Sankaranarayanan, S. K.; Cular, S.; Bhethanabotla, V. R.; Joseph, B. Flow induced by acoustic streaming on surface-acoustic-wave devices and its application in biofouling removal: A computational study and comparisons to experiment. *Phys. Rev. E* **2008**, *77* (6), 066308.
(22) Yeh, P.-Y. J.; Kizhakkedathu, J. N.; Madden, J. D.; Chiao, M. Electric field and vibration-assisted nanomolecule desorption and anti-biofouling for biosensor applications. *Colloids Surf., B* **2007**, *59* (1), 67−73.
(23) Vaidyanathan, R.; Rauf, S.; Shiddiky, M. J.; Trau, M. Tuneable surface shear forces to physically displace nonspecific molecules in protein biomarker detection. *Biosens. Bioelectron.* **2014**, *61*, 184−191.
(24) Meyer, G. D.; Morán-Mirabal, J. M.; Branch, D. W.; Craighead, H. G. Nonspecific binding removal from protein microarrays using thickness shear mode resonators. *IEEE Sens. J.* **2006**, *6* (2), 254−261.
(25) Cular, S.; Branch, D. W.; Bhethanabotla, V. R.; Meyer, G. D.; Craighead, H. G. Removal of nonspecifically bound proteins on microarrays using surface acoustic waves. *IEEE Sens. J.* **2008**, *8* (3), 314−320.
(26) Cui, W.; Zhang, H.; Zhang, H.; Yang, Y.; He, M.; Qu, H.; Pang, W.; Zhang, D.; Duan, X. Localized ultrahigh frequency acoustic fields induced micro-vortices for submilliseconds microfluidic mixing. *Appl. Phys. Lett.* **2016**, *109* (25), 253503.
(27) Chang, Y.; Tang, N.; Qu, H.; Liu, J.; Zhang, D.; Zhang, H.; Pang, W.; Duan, X. Detection of Volatile Organic Compounds by Self-assembled Monolayer Coated Sensor Array with Concentration-independent Fingerprints. *Sci. Rep.* **2016**, *6*, 23970.
(28) Liu, W.; Zhang, H.; Zhao, H.; Tang, Z.; Wang, Y.; Sun, C.; Pang, W.; Duan, X. Comparative analysis of static and non-static assays for biochemical sensing using on-chip integrated field effect transistors and solidly mounted resonators. *Sens. Actuators, B* **2017**, *243*, 775−783.
(29) Pang, W.; Zhao, H.; Kim, E. S.; Zhang, H.; Yu, H.; Hu, X. Piezoelectric microelectromechanical resonant sensors for chemical and biological detection. *Lab Chip* **2012**, *12* (1), 29−44.
(30) Zhao, H.; Guo, X.; Wang, Y.; Duan, X.; Qu, H.; Zhang, H.; Zhang, D.; Pang, W. Microchip based electrochemical-piezoelectric integrated multi-mode sensing system for continuous glucose monitoring. *Sens. Actuators, B* **2016**, *223*, 83−88.
(31) Nyborg, W. L. Acoustic streaming due to attenuated plane waves. *J. Acoust. Soc. Am.* **1953**, *25* (1), 68−75.
(32) Mitome, H. The mechanism of generation of acoustic streaming. *Electronics and Communications in Japan (Part III: Fundamental Electronic Science)* **1998**, *81* (10), 1−8.
(33) Collins, D. J.; Ma, Z.; Ai, Y. Highly localized acoustic streaming and size-selective submicrometer particle concentration using high frequency microscale focused acoustic fields. *Anal. Chem.* **2016**, *88* (10), 5513−5522.
(34) Collins, D. J.; Ma, Z.; Han, J.; Ai, Y. Continuous micro-vortex-based nanoparticle manipulation via focused surface acoustic waves. *Lab Chip* **2017**, *17* (1), 91−103.
(35) Friend, J.; Yeo, L. Y. Microscale acoustofluidics: Microfluidics driven via acoustics and ultrasonics. *Rev. Mod. Phys.* **2011**, *83* (2), 647.
(36) Zhang, Z.; Tang, Z.; Liu, W.; Zhang, H.; Lu, Y.; Wang, Y.; Pang, W.; Zhang, H.; Duan, X. Acoustically Triggered Disassembly of Multilayered Polyelectrolyte Thin Films through Gigahertz Resonators for Controlled Drug Release Applications. *Micromachines* **2016**, *7* (11), 194.
(37) Holmes, M.; Parker, N.; Povey, M. In *Temperature dependence of bulk viscosity in water using acoustic spectroscopy*, Journal of Physics: Conference Series, IOP Publishing, 2011; p 012011.

DOI: 10.1021/acssensors.7b00298
ACS Sens. XXXX, XXX, XXX−XXX

(38) Qi, Q.; Brereton, G. J. Mechanisms of removal of micron-sized particles by high-frequency ultrasonic waves. *IEEE transactions on ultrasonics, ferroelectrics, and frequency control* **1995**, *42* (4), 619−629.
(39) Lei, J.; Glynne-Jones, P.; Hill, M. Acoustic streaming in the transducer plane in ultrasonic particle manipulation devices. *Lab Chip* **2013**, *13* (11), 2133−2143.
(40) Sankaranarayanan, S. K.; Singh, R.; Bhethanabotla, V. R. Acoustic streaming induced elimination of nonspecifically bound proteins from a surface acoustic wave biosensor: Mechanism prediction using fluid-structure interaction models. *J. Appl. Phys.* **2010**, *108* (10), 104507.

DOI: 10.1021/acssensors.7b00298
ACS Sens. XXXX, XXX, XXX−XXX